The Insertion of the Antimicrobial Peptide Dicynthaurin Monomer in Model Membranes: Thermodynamics and Structural Characterization†

Frank Bringezu,*[,‡,#] Shaoying Wen,[‡] Silvia Dante,[§] Thomas Hauss,[§,||] Monika Majerowicz,[‡] and Alan Waring[⊥]

Institute of Medical Physics & Biophysics, University of Leipzig, 04107 Leipzig, Germany, Hahn Meitner Institute, Berlin Neutron Scattering Centre, 14109 Berlin, Germany, Institute of Physical Biochemistry, Darmstadt University of Technology, 64287 Darmstadt, Germany, and Departments of Medicine, University of California, Los Angeles, California 90095

Received January 23, 2007; Revised Manuscript Received March 16, 2007

ABSTRACT: This paper is focused on the thermodynamics and the structural investigation of the interaction of the antimicrobial peptide dicynthaurin monomer with model lipid membranes composed of mixtures of 1-palmitoyl-2-oleyl-glycerophosphocholine and -glycerophosphoglycerol. The thermodynamic binding parameters as obtained by isothermal titration calorimetry reveal strong binding toward the lipid model system dominated by large chemical binding constants which exceeds the electrostatic binding effects and thus suggests insertion of the amphipathic α-helical peptide into the hydrophobic membrane core. Circular dichroism study shows that the peptide exhibits trans-membrane α-helix secondary structure. Neutron diffraction measurements using partially deuterated sequences were successfully applied to determine the orientation of the peptide thus proving insertion into the hydrophobic membrane core. This insertion and the formation of higher order porelike aggregates is assumed to be the most relevant event in microbial membrane perturbation that *in vivo* finally leads to bacterial cell death on a fast time scale.

Antimicrobial peptides (AP) have been identified as being the native line of defense throughout Nature, e.g., in animals, plants, and also single-cell organisms. The immune response is governed by the expression of the peptides that show a high toxicity against diverse species including both Gram-negative and Gram-positive bacteria, but they often also exhibit activity against fungi, and some also show antiviral activity (*1*−*4*). A wealth of active sequences has been described; most of them are relatively short length peptides with fewer than 100 amino acid residues forming diverse structures. A high content of mostly positively charged residues in polar side chains leads to amphipathic structural elements. The increasing scientific interest on the antimicrobial activity is mainly driven by the relevance of the AP's to intrinsic host defense and the enormous potential in future drug development (*5*). There is a strong line of evidence that the activity of many AP's is directly connected with the interaction between the peptides and the membrane bilayer (*6*). This interaction between the positively charged peptide and the negatively charged bacterial membrane affects the integrity of the bacterial cell by forming pores, inducing curvature or disrupting the membrane which finally leads to cell death. For the process, different mechanisms have been proposed in the literature (*7*−*9*).

In recent studies, a novel antimicrobial peptide, dicynthaurin, was isolated from the hemocytes of a tunicate, *Halocynthia aurantium*. Dicynthaurin belongs to a unique group of amphipathic α-helical antimicrobial peptides from tunicates. These peptides include halocidin (*10*, *11*) and dicynthaurin (*12*); both peptides have an unusual structural motif consisting of two amphipathic helices that are covalently linked through a single disulfide bond formed between adjacent single cystine residues. For dicynthaurin, in a membrane mimetic environment an α-helical secondary structure was found for both the peptide monomer and the dimer, respectively. Dicynthaurin's broad spectrum activity encompassed Gram-positive (*Micrococcus luteus*, *Staphylococcus aureus*, *Listeria monocytogenes*) and Gram-negative bacteria (*Escherichia coli*, *Pseudomonas aeruginosa*), but not *Candida albicans*, a fungus. Comparing the activity of the monomer and the cynthaurin dimer, the dimer shows better response; however, on a weight basis the activity was found equivalent (*12*). The native peptide is composed of two mono-cystine-bounded monomers (I L Q K A V L D C L K A A G S S L S K A A I T A I Y N K I T) of 30 amino acids with a formal positive charge of +3. From the peptide sequence it is clearly evident that, for the monomer, clustering of polar and apolar residues imparts amphipathicity, thus suggesting a high capacity for membrane insertion.

In a recent work, the binding of dicynthaurin monomer with lipid model membranes has been extensively studied by isothermal titration calorimetry (ITC[1]) (*13*) using the sequence that contains alanine instead of cysteine to avoid

† This work was supported by the Deutsche Forschungsgemeinschaft (Emmy Noether Grant BR 1826/2-4).

* Corresponding author. Mailing address: Institute of Medical Physics and Biophysics, University of Leipzig, Härtelstrasse 16-18, 04107 Leipzig, Germany. E-mail: bringezu@denet.de. Tel: +49-341-9715726. Fax: +49-341-9715709.

‡ University of Leipzig.

Current address: MZP, Inst. of Biotechnology, Martin Luther University, Halle-Wittenberg, 06120 Halle, Germany.

§ Berlin Neutron Scattering Centre.

|| Darmstadt University of Technology.

⊥ University of California, Los Angeles.

[1] Abbreviations: ITC, isothermal titration calorimetry; DLS, dynamic light scattering; CD, circular dichroism; POPC, 1-palmitoyl-2-*sn*-oleoyl-glycero-3-phosphatidylcholine; POPG, 1-palmitoyl-2-oleoyl-*sn*-glycero-3-phospho-*rac*-(1-glycerol)] (sodium salt).

10.1021/bi7001295 CCC: $37.00
Published on Web 04/24/2007

spontaneous dimerization. The ITC analysis using a surface partitioning equilibrium model shows that the interaction is predominately driven by hydrophobic effects (K_b between 2×10^4 and 1×10^5 M^{-1}). The improved in vivo activity of the peptide at low salt conditions is mainly due to the enhanced electrostatic interaction leading to larger peptide concentrations immediately above the vesicle surface, which initiates the further insertion of the peptide more effectively. Fluorescent leakage measurements have shown the leakage of the fluorescent dye induced by the peptide. From the leakage kinetics analysis a minimum aggregation number of about 7 ± 2 peptide monomers per pore is obtained. The DLS measurements confirm the maintained integrity of the vesicle. Such findings also suggest that the fluorescent leakage found in the model system is initially driven by pore formation (*13*). As pore formation requires aggregation of surface bound peptides, the dimer sequence in dicynthaurin offers the advantage of having already two monomer units bound in a single binding event. This could help to improve the antimicrobial activity; but on the other hand, such dimerization could also alter the mechanism of membrane perturbation as the dimer could exhibit a more polar peptide surface while the monomer shows amphipathic properties. For melittin recent X-ray diffraction studies showed small perturbations for the peptide monomer; however, a cysteine-substituted melittin causes much larger structural changes under equivalent conditions, suggesting that self-association of amphipathic helices maybe the crucial step toward membrane lysis (*14*).

The orientation of helical peptides bound to lipid bilayers has been examined in great detail by many investigators. For melittin and alamethicin it was shown that the orientation of the helix axis varies depending on the physicochemical conditions of the bilayers. From spectroscopy and CD data it was concluded that both peptides are oriented preferentially parallel to the membrane normal at high water content. However, upon cooling the samples below the main transition temperature, the peptides' long axis moves toward the membrane plane. For low water content, a parallel orientation (perpendicular to the membrane normal) of the helices was suggested (*15*, *16*). Huang and co-workers have found that the most important parameter for controlling the peptides' orientation at constant physicochemical environment is the peptide/lipid (P/L) ratio. Using a combination of CD and neutron diffraction measurements on oriented samples, for melittin they have observed a parallel orientation of the helix to the bilayer below a certain peptide threshold concentration. With increasing P/L ratio, the helix orientation starts to move toward the surface normal, and above a critical concentration all peptide molecules exhibit such a perpendicular orientation (*17*). This change in orientation is strongly dependent on the lipid composition of the bilayer and was most pronounced for POPC. In this perpendicular orientation, pore formation has been observed for both alamethicin and melittin; however, from the analysis of the single channel conductance of alamethicin, a barrel stave model was derived, where the channel changes its conductivity when a single peptide enters or leaves the pore (*18*). The absence of such discrete levels in the ion conductivity measurements performed on the antimicrobial peptide magainin (*19*) together with crystallographic data (*20*) and neutron results strongly suggest that these peptides form pores that are described with the toroidal model (*17*).

Despite published knowledge about the interaction of dicynthaurin monomer with model monolayers (*21*, *22*) and bilayers (*13*), direct evidence about the penetration of the peptide in the membrane and its location and orientation thereafter has not yet been obtained. In this paper we have applied isothermal titration calorimetry (ITC) in order to get information about the thermodynamic parameters of the binding of the dicynthaurin monomer to lipid model membranes closely mimicking the phospholipid composition of a bacterial cytoplasmic membrane. A circular dichroism study has been performed to gain information about the secondary structure change of the peptide before and after exposure to the lipid membrane. Additionally, neutron diffraction measurements using partially deuterated peptides have been applied to elucidate the peptides' orientation and location in model membranes using supported lipid bilayers on solid substrates. The data obtained demonstrate that the peptide strongly binds and inserts into the membrane. The CD study has revealed a trans-membrane distorted α-helical secondary structure upon interaction with the model membrane. Neutron diffraction demonstrates that the peptide is located in the hydrophobic core of the membrane by crossing through the bilayer which is also found in our simulations. The findings described in this paper strongly support our former assumption that a pore formation is the underlying mechanism of the antimicrobial activity.

MATERIALS AND METHODS

Materials. The 30 amino acid dicynthaurin monomer was prepared at a 0.25 mmol scale on an ABI 431A peptide synthesizer using FastMoc chemistry and further purified by RP-HPLC. Using deuterated alanine for the peptide synthesis yielded a partially deuterated sequence carrying the isotopic labeled amino acid at the fifth position. The molar masses were confirmed using MALDI-TOF and electrospray mass spectrometry (UCLA Center for Molecular and Medical Mass Spectrometry, Los Angeles, CA). For the ITC experiments a peptide sequence that contains an alanine instead of cysteine residue was used in order to avoid spontaneous dimerization. The deuterated peptide samples did contain the cysteine present also in the native sequence. Here, MALDI-TOF analysis of the lipid−peptide dispersion before and after the measurements indicated that the peptide remained in a reduced monomeric state.

1-Palmitoyl-2-oleoyl-*sn*-glycero-3-phosphocholine (POPC) and 1-palmitoyl-2-oleoyl-*sn*-glycero-3-[phospho-*rac*-(1-glycerol)] (sodium salt) (POPG) were purchased from Avanti Polar Lipids and used as obtained without further purification. ITC samples are prepared in phosphate buffered saline solution (PBS) containing 10 mM phosphate with 140 mM NaCl at pH 7.4. All aqueous solutions were prepared using Milli-Q deionized water of a specific electrical conductivity of >18 MΩ cm.

For the experiments, peptide stock solutions were prepared by dissolving the solid peptide in PBS followed by vortexing for 10 min. For the preparation of the lipid mixtures certain amounts of POPC and POPG (3/1 mol/mol) were mixed via organic solvents and consecutively dried under a stream of nitrogen. Cyclohexane was used for subsequent dissolving

the lipid film to lyophilize by freeze-drying overnight. Finally the dry solid mixture was weighed and suspended in PBS by intensive vortexing followed by five freeze−thawing cycles. The lipid concentration was determined on a weight basis of the dry powder. All samples were stored at 4 °C prior to usage. For the neutron diffraction study, the sample preparation was performed using Milli-Q water as solvent.

Methods. Titration Calorimetry. The experiments were performed using an isothermal titration calorimeter VP-ITC (Microcal Inc., Northampton, MA). For the analysis the dilution data of either lipid to buffer or peptide to buffer experiments were subtracted from the binding heat obtained in the lipid to peptide. Initial data analysis (background subtraction, peak integration) procedures were performed using the MicroCal Origin 5.0 software package. In the lipid to peptide titration experiment, a 5 mM lipid solution was titrated into the sample cell, which contains 1.4337 mL of peptide solution at a concentration of 40 μM. The first injection is subject to the largest errors caused mainly by injection volume variations, and therefore, an injection sequence ($1 \times 1\ \mu L + n \times 5\ \mu L$) was applied to limit the influence of the possible errors present in this first titration step on the further analysis. Final ITC data given in this paper were repeated at least three times. To fit the heat traces we adopted the data handling program that comes with the ITC device. For further analysis, the surface partitioning model was applied using a fitting procedure programmed in IDL (Research Systems Inc., Boulder, CO) (*23*, *24*). In brief, it describes the peptide−lipid interaction by means of a partitioning equilibrium of free and bound peptide between the aqueous phase and the surface of the liposome. The apparent binding constant/partitioning equilibrium constant is defined as

$$K_{app} = \frac{P_b/\gamma L}{P_{free}} = \frac{P_b/\gamma L}{P - P_b} = K_b \exp\left(-\frac{Z_p F \psi_0}{RT}\right) \quad (1)$$

where γ is the accessibility of lipid molecules to the peptide; P, P_b, and P_{free} are the total concentration of peptide, the concentration of peptide bound to the membrane surface, and the unbound peptide, respectively; L is the total lipid concentration; and K_b is the intrinsic binding constant, which describes the chemical binding. The exponential part of K_{app} describes the electrostatic interaction. Z_p denotes the effective charge of the peptide, and ψ_0 denotes the surface potential of the liposome. The detailed description about this model is presented elsewhere (*23*, *24*).

Circular Dichroism Measurements. Circular dichroism spectra were recorded with a Jasco 720 (JASCO Inc., MD) spectrophotometer from 190 to 260 nm using quartz cuvettes with an optical path length of 0.1 cm, peptide concentration of 0.2 mg/mL, and POPG liposome concentration of 1 mM. The data were obtained after accumulation of four measurements for PBS and 8 measurements for all other samples investigated using a speed of 50 nm/min, a response of 2 s, a bandwidth of 1.0 nm, and a data pitch of 0.2 nm. The analysis was performed after subtraction of the spectra of the corresponding subphase (PBS or POPG liposome in PBS) using mean residual molar ellipticity, [θ].

Neutron Diffraction Measurements. The diffraction measurements were carried out using the V1 membrane diffractometer at the Berlin Neutron Scattering Centre (BENSC) in the Hahn Meitner Institute (HMI, Berlin, Germany). Oriented samples were obtained by spreading aqueous dispersions of the lipid mixtures onto quartz glass slides ($65 \times 15 \times 0.3$ mm) and subsequent solvent evaporation for 24 h in a dust free environment at room relative humidity and ambient temperatures and finally dried in a vacuum desiccator over 12 h. For the peptide containing samples, a certain amount of the aqueous peptide stock solution was added to the lipid dispersion before spreading. For the experiments, the samples were rehydrated for 24 h at room temperature in a fully hydrated atmosphere of 98% relative humidity maintained with a saturated K_2SO_4 solution. Each sample contained about 10 mg of lipid and different molar concentrations of partially deuterated peptide. Contrast variation was achieved by adjusting the atmosphere in the sample chamber at three different $H_2O/^2H_2O$ compositions (50, 20, and 8 vol % ^2H_2O). For the measurement the samples were vertically mounted and placed in an aluminum chamber. The diffraction intensities were measured up to the 5th order of the lamellar spacings at 20 °C using rocking scans around the expected Bragg positions with exposure times between 20 min and 4 h depending on the scattered intensities.

For data analysis, the lamellar spacing d was determined from the 2θ values of the reflections using the Bragg equation. The structure factor amplitudes $|F(h)|$ are obtained from the square rooted integral of the Gaussian fit to the diffraction peak followed by correction for absorption and Lorentz factor. The relative absolute density profile $\rho(z)$ is

$$\rho(z) = \rho_0 + \frac{2}{d}\sum_{h=1}^{n} F(h) \cos\left(\frac{2\pi h z}{d}\right) \quad (2)$$

where F is in units of the scattering length and ρ_0 is the average scattering length per unit length of the bilayer. $F(h)$ are the scaled structure factors, and the sum describes the distribution in scattering length across the bilayer. Isomorphous replacement using $^2H_2O/H_2O$ exchange allowed phase assignment, as the structure factors are linearly related to the $^2H_2O/H_2O$ ratios. Structure factors for all samples were measured at three different isotopic water vapor compositions. For the localization of the deuterium label, measurements at 8% ^2H_2O are taken into account, because at these conditions the water layer depicts zero scattering length density. For further information we kindly refer to the literature (*25*−*27*).

RESULTS AND DISCUSSION

To get information about the binding equilibrium of the peptide toward vesicles consisting of a lipid mixture of negatively charged POPG and neutral POPC in 1/3 molar ratio, we have applied ITC experiments titrating the vesicle suspension into the peptide solution. Figure 1 (top) shows the titration curve exhibiting exothermic binding events that decrease in intensity with ongoing titrations as the peptide binds to the lipid and consequently the free peptide concentration is reduced. The integration of the heat flow vs time curve gives the binding isotherm, i.e., molar heat of binding per lipid molecule as function of the lipid/peptide molar ratio (see Figure 1, bottom). Here, the solid line depicts the fit using the surface partitioning equilibrium model (*23*, *24*). This analysis yields the intrinsic binding constant (K_b), the

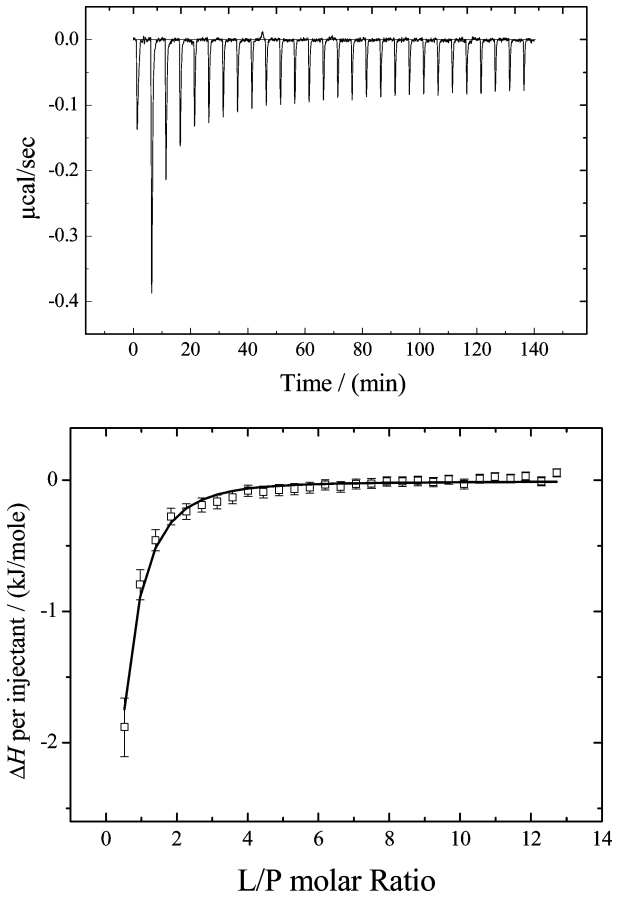

FIGURE 1: Calorimeter tracings (heat flow vs time) of a titration of POPC/POPG (3/1 mol/mol) vesicles (5 mM, 2.5 μL) into dicynthaurin monomer solution (40 μM). The experiment was performed in phosphate buffer (10 mM phosphates, pH = 7.4, 140 mM NaCl) at 45 °C. The lower panel shows the integrated and normalized heat from this ITC experiment, and the solid line represents the fit result using the surface partitioning equilibrium model.

effective peptide charge (Z_p), and the molar binding enthalpy per bound peptide (ΔH_b) of $(1.6 \pm 0.5) \times 10^5$ M^{-1}, 0.5, and (-2.1 ± 0.3) kJ/mol, respectively. For this calculation, the accessibility of the liposome of 0.6 was taken into account. The small exponential term of only 1.2 obtained in the analysis is much smaller than the intrinsic binding constant. Such behavior has also been found previously for a series of POPC/POPG mixtures (*13*). The molar binding entropy calculated from these data suggests an entropy driven binding mechanism as the $T\Delta S_b$ value is about 20-fold of the binding enthalpy. Both findings, the large intrinsic binding constant and the entropy driven process, can be explained by the classical and nonclassical hydrophobic effects, e.g., water release from the peptide upon binding and membrane incorporation of the peptide in the hydrophobic bilayer core (*28*−*30*). In addition, a change in the peptides secondary structure upon binding or insertion would also contribute to such an effect.

To study the effect of membrane binding on the formation of the secondary structure, we have undertaken CD measurements on the peptide in PBS and in a POPG suspension (C_L = 1 mM). Figure 2 plots the mean residual molar ellipticity of the peptide showing the typical minima of negative ellipticity at about 220 and 205 nm and positive ellipticity at 192 nm suggesting mainly α-helical content.

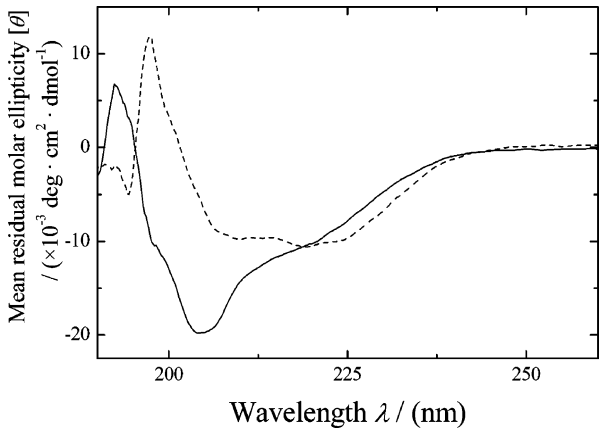

FIGURE 2: CD spectra of dicynthaurin monomer performed in 10 mM phosphate buffer containing 140 mM NaCl (solid) and in POPG vesicle solution (1 mM, dotted) recorded at 20 °C.

For the analysis of the CD data in terms of the secondary structure content, we have applied CDPRO, which has been successful in estimating the secondary structure of membrane proteins (*31*, *32*). The pure peptide contained about 40% α-helical content corresponding to 12 amino acids with some minor contributions coming from unstructured peptide sequence. The CD spectrum obtained after adding the peptide to POPG vesicles in PBS also depicts typical features of α-helical components, but the maximum position of the positive ellipticity moved toward larger wavelength (λ = 198 nm) and the negative ellipticity at 205 nm shifts toward larger λ-values and is less pronounced, features that are typically found for a trans-membrane α-helix (*33*, *34*).

To get information about structural changes that occur upon peptide binding and about the orientation of the peptide in the bound state, we have studied the lipid mixture on solid support before and after peptide incubation by means of low angle neutron diffraction measurements. Figure 3 depicts the rocking curves around the first-order Bragg reflections obtained for the pure lipid and subsequent mixtures with dicynthaurin monomer in different concentrations. The pure lipid shows a narrow mosaicity, i.e., a well-aligned lipid bilayer orientation with respect to the surface normal determined by the quartz support. Adding peptide to the lipid system increases the peak width of the diffracted intensities in the ω-direction, thus indicating a perturbation of the lipid bilayer orientation by the peptide. This effect becomes more dominant with increasing peptide concentration. At 1 mol %, the region of narrow mosaicity around the first-order Bragg position remains present, but at the largest peptide concentration investigated (3 mol %), a typical powder diffraction pattern is observed and the narrow mosaicity around the first-order Bragg position is completely disappeared.

Figure 4 summarizes the 2θ-integrated rocking scans showing a sharp signal of the pure lipid (A) with a fwhm of about 0.36°, a value that is typically found for well-aligned lipid samples (*27*). On adding the peptide to the model system, the signal obtained cannot be sufficiently described by a single Gaussian peak, but instead larger deviations have to be taken into account that indicate a portion of the stacked bilayers that is clearly influenced by peptide. At 1 mol % peptide (C), a more homogeneous intensity distribution in the whole omega region and significant smaller intensities

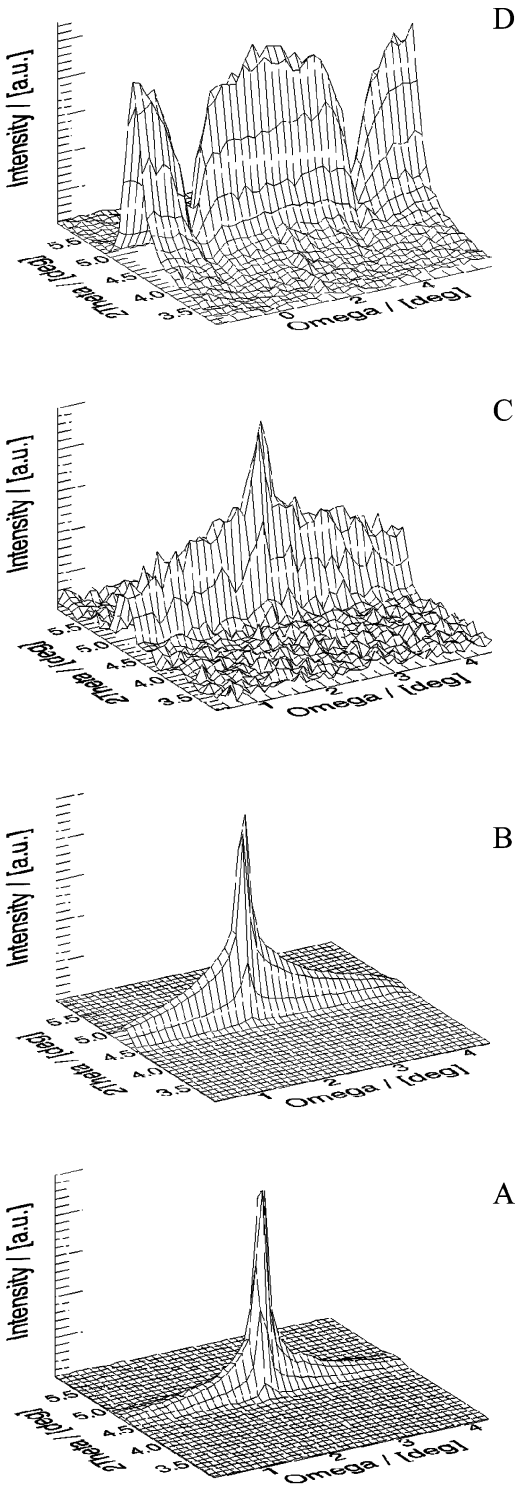

FIGURE 3: Rocking curves obtained at 8% ^2H_2O contrast by rotating the samples around the first-order Bragg reflection with an angle of $\omega = \pm 2°$. Panel A shows a narrow reflection of the well-aligned pure lipid sample. Adding dicynthaurin monomer drops the intensity of this sharp peak (B, 0.3 mol %; C, 1.0 mol %; D, 3 mol %). The upper panel shows a long range ($\omega \pm 20°$) rocking scan with the two dips representing the adsorption maxima of the samples respectively.

at the Bragg peak position are obtained. Figure 4 (D) shows the integrated wide range rocking curve ($-18° < \omega < 22°$) obtained for the mixture containing 3 mol % peptide. The region of narrow mosaicity is completely disappeared, and a broad Gaussian distribution (fwhm = 30°) that describes the bilayer disorientation induced by the peptide is obtained.

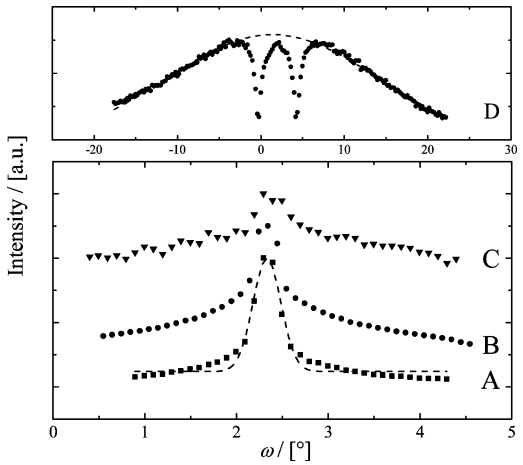

FIGURE 4: The 2θ-integrated rocking profiles of the POPC/POPG (3/1 mol/mol) lipid mixture before (A) and after peptide exposure at different molar concentrations of 0.3% (B), 1.0% (C), and 3% (D), along with the Gaussian fits to the pure lipid (A) and the powderlike pattern observed after dicynthaurin monomer incorporation (D: 3 mol %). The patterns were determined at 8% ^2H_2O contrast.

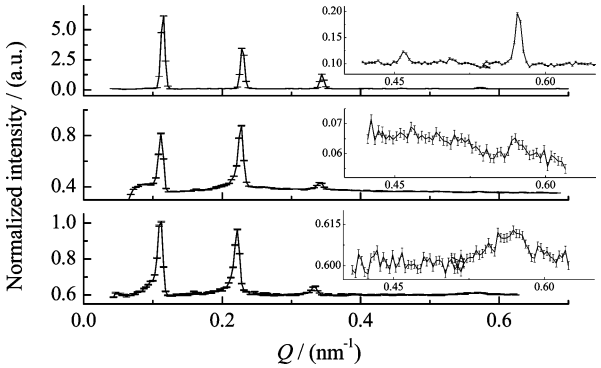

FIGURE 5: From top to bottom, the diffraction patterns of the pure lipid mixture (POPC/POPG 3/1 mol/mol) and subsequent mixtures with dicynthaurin monomer (3 mol %) and with 5-Ala-^2H dicynthaurin monomer are summarized. For clarity the fourth and fifth order of each profile are presented in the corresponding insets at a different *y*-scale. The patterns were determined at 8% ^2H_2O contrast.

The Bragg diffraction peaks recorded for the pure lipid system (top) and the lipid model containing 3 mol % of protonated (middle) and deuterated (bottom) peptide are shown in Figure 5. For the pure lipid system, five Bragg peaks of a lamellar structure can be resolved. From the peak maximum positions a spacing of (55 ± 0.2) Å can be calculated. The lamellar spacing calculated from the peak positions after adding 3 mol % peptide amounts to (54.9 ± 0.2) Å, indicating that the overall membrane thickness is not significantly affected by the peptide. However, the change in the intensity distribution points to a modification of the structure factors and moreover to an alteration of the neutron scattering length density profiles.

The analysis of the diffraction patterns yields structure factors that allow calculating the neutron scattering length density profiles. Figure 6 shows the result obtained for the pure lipid model. The profile depicts the typical features expected for a lamellar lipid structure, e.g., two maxima for the highest scattering density at the lipid head group regions and a minimum of lowest scattering density at the terminal CH_3 groups in the membrane core. The two shoulders between maximum and minimum represent the alkyl chain

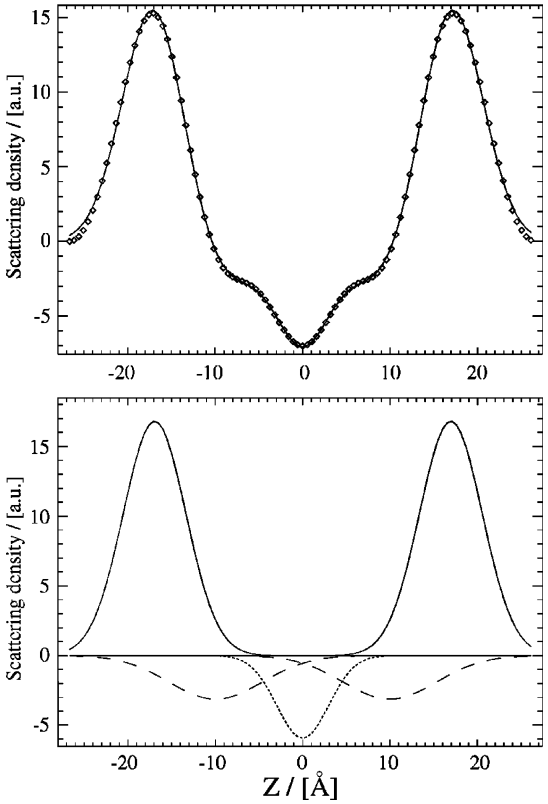

FIGURE 6: Neutron scattering length density profile calculated from the measured structure factors of a POPC/POPG (3/1) bilayer along the bilayer normal (◇). The lower panel depicts the decomposition of the profile into Gaussian peaks representing different submolecular groups: polar heads (solid), alkyl chains (dashed), and methyl groups (dotted). The solid line in the upper panel depicts the best fitting result using the Gaussian peaks for these submolecular groups respectively. The profile was determined at 8% ^2H_2O contrast.

Table 1: Fit Parameters of the Gaussian Peaks Representing Different Submolecular Groups as Shown in Figure 6

gauss	area per Gaussian	position/(Å)	width/(Å)
peak A (4 × CH_3 groups)	−44.0 ± 0.5	0	5.9 ± 0.2
peak B (2 × alkyl chains)	−41.9	10.0 ± 0.3	10.7 ± 0.4
peak C (head group incl glycerol backbone)	151.2	16.9 ± 0.8	7.2 ± 0.2

regions of the hydrophobic part of the molecules that contain the single double bond in each oleyl chain. A more quantitative description of the data was achieved by decomposition of the profile into the individual contributions arising from the head groups, the chain regions, and the four terminal CH_3 groups (see Figure 6, bottom) coming from the two lipid molecules, respectively. To limit the number of free parameters during refinement, the mirror symmetry of the system was taken into account. Given the chemical structure of the molecule, the scattering length per molecular group can be calculated, thus allowing the area ratio of the Gaussian peaks to be kept at fixed values that reflect the scattering length ratios accordingly. Using this approach, six parameters are taken into account, i.e., two positions of the head group and the chain part respectively, three widths of each Gaussian peak, and one scaling factor for the area. The solid line in Figure 6 (top) depicts the global fit result. From the fitted width of the Gaussian peaks (see Table 1), a length per lipid

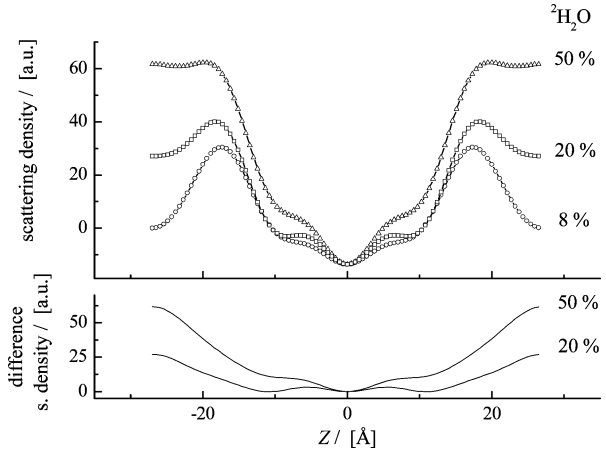

FIGURE 7: Density profiles of the pure lipid bilayer at all ^2H_2O contrasts measured. Increasing ^2H_2O content from 8 to 50% in the water composition shifts the profiles in the head group region to larger values. The lower panel depicts the difference of the profiles given to the profile obtained at 8% ^2H_2O.

molecule of 20.9 Å can be calculated, which includes about 13.7 Å for the hydrocarbon region, a small value that reflects molten chains.

The scattering length density profiles obtained for the pure lipid mixture at different $H_2O/^2H_2O$ contrasts are given in Figure 7. Increasing the ^2H_2O content in the atmosphere increases the scattering length density in all molecular subunits that are hydrated, in particular at the lipid head groups. Starting from 8% ^2H_2O, the water bound to the lipid head groups depicts zero scattering length density. On going from 8 to 20% ^2H_2O, the profile exhibits larger values at the head group region and the water layer between opposing bilayers. Additional lift up at the hydrophobic membrane core suggests some hydration also at the methylene groups of the oleyl chains. Further increase in the ^2H_2O content shows pronounced shifts in the scattering length densities at the relevant positions. The superior hydration at the lipid head groups yields a shift of almost the whole profile that extends deep into the chain region, thus making the slight hydration at the methylene groups relatively less pronounced. However, the difference in the density profiles shown in the lower panel clearly depicts the additional hydration at the methylene groups besides the lipid head groups present in both difference profiles.

The difference of the profiles yields the remaining scattering length density that must be attributed to the change in the ^2H_2O content of the hydrating atmosphere, thus allowing calculation of the number of water molecules bound per lipid molecule. From the calculated scattering length density of 20% and 50% ^2H_2O, the number of water molecules bound to one lipid molecule amounts to 17 ± 2, respectively indicating full hydration under the experimental conditions (*35*). Fitting the difference of the profiles (see Figure 7, bottom) with two Gaussians per lipid molecule gives a very good description of the experimental finding, thus allowing division of the total number of bound water molecules into 16 mol of water associated with the lipid head group and 1 mol penetrating into the hydrophobic part.

Figure 8 (top) shows the profile calculated from the diffraction pattern of the lipid containing 3 mol % dicynthaurin monomer. Taking the profile obtained for the pure lipid into account (see Figure 6), peptide addition yields a

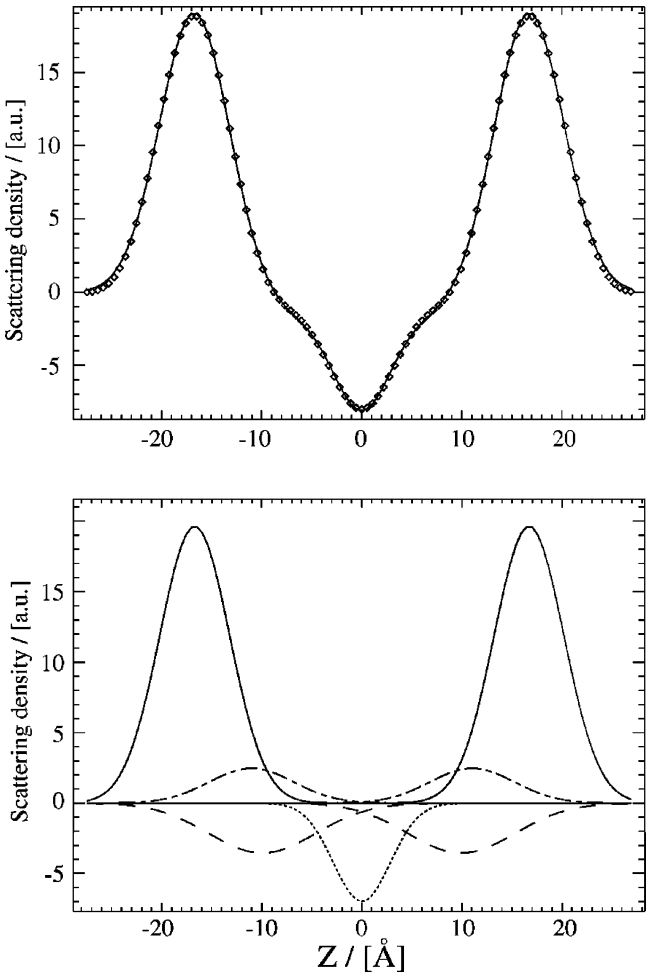

FIGURE 8: Neutron scattering length density profile calculated from the measured structure factors of a POPC/POPG (3/1) bilayer containing 3 mol % dicynthaurin monomer (◇). The lower panel depicts the decomposition of the profile into Gaussian peaks representing different submolecular groups of the pure lipid: polar heads (solid), alkyl chains (dashed), methyl groups (dotted), and the residual scattering length density (dash dotted). The solid line in the upper panel depicts the best fitting result using the Gaussian peaks for these submolecular groups respectively. The profile was determined at 8% ^2H_2O contrast.

smearing out effect in the membrane core region. The peptide sequence shows a positive scattering length as its chemical composition contains large amounts of carbon, nitrogen, and oxygen. Figure 8 (bottom) shows the decomposition of the profile into the pure lipid and the remaining residue of the lipid/peptide profile. The positive residual scattering length in the central part of the membrane could be attributed to the insertion of the peptide showing positive scattering length. However, a simple additive effect of scattering lengths from pure lipid and the peptide is unlikely, instead also a change of the lipid structure must be taken into account.

Detailed information about the location of the peptide is derived from the comparison of the two samples containing labeled and unlabeled dicynthaurin monomer. Figure 9 exhibits the neutron scattering length density profiles obtained from protonated (solid) and partially deuterated peptide (^{2}H-Ala-5, dashed) at 8% ^2H_2O. The difference between these two density maps (dotted) yields the deuterium distribution in the lipid bilayers showing three maximum positions in a centrosymmetric unit cell. Fitting Gaussian functions to the

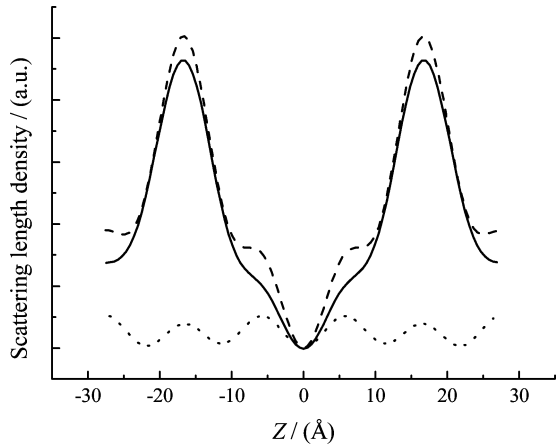

FIGURE 9: Neutron scattering length density profiles of POPC/POPG (3/1) mixture containing 3 mol % dicynthaurin monomer (solid) and the lipid mixture containing 3 mol % ^{2}H-Ala-5 dicynthaurin monomer (dashed). The dotted line represents the difference between the two profiles. The profiles were determined at 8% ^2H_2O contrast.

^{2}H-distribution curve yields the amount of deuterium located in the membrane: 46% in the membrane core and 35% bound at the lipid head groups. The aqueous medium contains only 19% of the deuterium available. Insertion into the hydrophobic core of the membrane requires adsorption to be an initial step before insertion can take place. The large amount of deuterium detected at the membrane core region suggest that the peptide has a high capability to insert into the membrane, which is in general agreement with the findings from both ITC and CD measurements. However, the large peptide concentration of 3 mol % required for the detection of deuterium might also be larger than the saturation of the insertion, thus a significant amount of peptide remains in the aqueous bulk between adjacent headgroups. This would explain the large value found for deuterium present in the aqueous phase. In recent studies on melittin binding toward POPC membranes, a concentration dependent orientation of the α-helical peptide was found for fully hydrated bilayers. At a P/L ratio of 1/40, 85% of the peptides are oriented parallel to the bilayer, and at a larger peptide concentration of P/L = 1/15, more than 60% of the peptides are aligned parallel to the bilayer normal (*17*). Such behavior could also be relevant for our system showing a P/L ratio of about 1/32 and thus explain the findings from the neutron scattering length density profile (Figure 9) by equilibrium of peptides oriented along the bilayer normal (e.g., inserted into the membrane core) and substantial amounts of the peptide molecules oriented perpendicular (e.g., parallel to the bilayer surface); the latter would cause the increase in scattering length density at the membrane surface.

The activity profile of dicynthaurins exhibits a maximum at low salt conditions suggesting predominantly intracellular function (*12*). Changing the salt concentration alters the interaction between the peptide and the lipid as shown in a recent ITC study. The results clearly show a change in the electrostatics of the interaction, thus a change in the distribution of the peptide between water, headgroup, and lipid core must be taken into account. Therefore, it would also be interesting to study the effect of changing salt concentration or pH on the peptide distribution within the

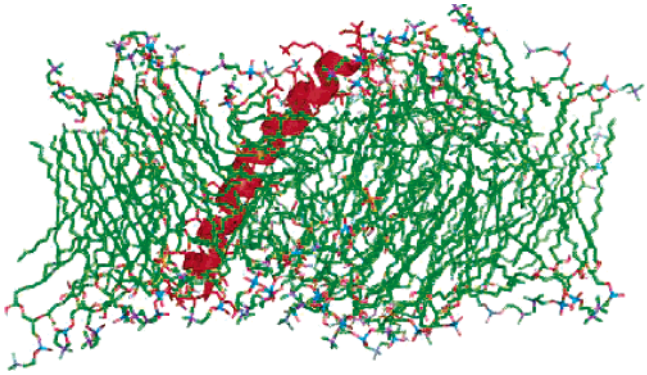

FIGURE 10: Computer molecular graphics cross-sectional representation of the trans-membrane insertion of dicynthaurin monomer in a POPC/POPG (3/1 mol/mol) bilayer ensemble obtained using a preoptimized peptide structure that was embedded into a lipid bilayer followed by minimization steps as described in the text.

bilayer, which would provide additional evidence for the pore formation mechanism as proposed (*13*).

Figure 10 depicts a computer molecular graphics cross-sectional representation of the trans-membrane insertion of dicynthaurin monomer in a bilayer ensemble composed of a lipid mixture of POPC/POPG = 3/1 mol/mol with the water molecules removed for clarity. The amino acid sequence was modeled as an α-helix conformation using Hyperchem 7.5 (http://www.hyper.com). This initial peptide conformation was then inserted into a pre-equilibrated bilayer by carefully removing several lipid molecules from each side of the model membrane (*36*). The peptide−lipid bilayer ensemble was then optimized using the Inflategro utility (http://moose.bio.ucalgary.ca) in the GROMACS version 3.3.1 environment (*37*). After optimization of the ensemble, the system was hydrated in a (64 × 64 × 64) Å^3 solvent simulation box. The system was then subjected to steepest descent minimization followed by 10 ps of dynamics at 25 °C with the peptide constrained and an unrestrained dynamics for 1 ns to approximate an apparent equilibrium-like state. The computer graphic illustration of the dynamics run was then rendered using PyMOL v0.99 (http://pymol.sourceforge.net). After finishing the 1 ns simulation, the α-helical peptide spans through the membrane and adopts a tilted orientation within the bilayer. However, the tilt of the peptide suggests that under equilibrium conditions several different types of orientations in the lipid environment showing flexibility in the tilt must be taken into account. Upon accumulation of more peptide monomers spanning through the membrane, higher order porelike structures could form that stabilize the orientational flexibility of a single peptide monomer found in our preliminary simulations. The result of the simulation showing the peptide spanning through the membrane strongly supports our experimental findings from the neutron diffraction and the CD study. The formation of higher order aggregates or pores as suggested experimentally by fluorescent leakage measurements remains to be explored in the simulations.

CONCLUSION

The large amount of deuterium present in the membrane core strongly suggests that the peptide is inserted into the bilayer. Such a membrane insertion would be a prerequisite for pore formation, one of the main mechanisms for antimicrobial peptide mode of action. On the other hand, insertion would modify the energy balance for the binding, favoring intrinsic contributions over electrostatic effects; the latter would facilitate initial peptide accumulation at the lipid head groups. The location of the peptide being inserted into the membrane core is in very good agreement with the large intrinsic binding constant found in the ITC study on this particular lipid system, but also for lipid mixtures at different PC/PG ratios. In addition, the trans-membrane helix structural motive present in the CD measurements and the constant *d*-value obtained in the neutron diffraction measurements also support the high insertion capability of the peptide. This inserted peptide is probably in equilibrium with surface bound peptide showing a parallel alignment, a behavior that was also found for melittin binding toward POPC (*17*). Therefore, we can conclude that the dicynthaurin monomer binds to phospholipids typically found in bacterial cytoplasmic membranes and shows strong insertion capacity, thus being able to form a trans-membrane pore. This pore formation would disturb the integrity of the microbial cell. The dissipation of ion and water gradients across the disrupted membrane must be continuously compensated by the microbes thus leading a cumulative energy drain and a loss in viability that finally kills the target microbes on a short time scale.

ACKNOWLEDGMENT

We gratefully acknowledge C. Olak for support during CD experiments and Dr. G. Brezesinski for helpful discussions and experimental support.

REFERENCES

1. Boman, H. G., Marsh, J., and Goode, J. A. (1994) *Antimicrobial Peptides*, John Whiley and Sons, Chichester.
2. Wu, Z. B., Cocchi, F., Gentles, D., Ericksen, B., Lubkowski, J., DeVico, A., Lehrer, R. I., and Lu, W. Y. (2005) Human neutrophil alpha-defensin 4 inhibits HIV-1 infection in vitro, *FEBS Lett. 579*, 162−166.
3. Owen, S. M., Rudolpil, D. L., Wang, W., Cole, A. M., Waring, A. J., Lal, R. B., and Lehrer, R. I. (2004) RC-101, a retrocyclin-1 analogue with enhanced activity against primary HIV type 1 isolates, *AIDS Res. Hum. Retroviruses 20*, 1157−1165.
4. Hancock, R. E., and Scott, M. G. (2000) The role of antimicrobial peptides in animal defenses, *Proc. Natl. Acad. Sci. U.S.A. 97*, 8856−8861.
5. Hancock, R. E. W. (2000) Cationic antimicrobial peptides: towards clinical applications, *Expert Opin. Invest. Drugs 9*, 1723−1729.
6. Lohner, K. (2001) The role of membrane lipid composition in cell targeting of antimicrobial peptides, in *Development of Novel Antimicrobial Agents: Emerging Strategies* (Lohner, K., Ed.) pp 149−165, Horizon Scientific Press, Norfolk.
7. Matsuzaki, K., Sugishita, K., Ishibe, N., Ueha, M., Nakata, S., Miyajima, K., and Epand, R. M. (1998) Relationship of membrane curvature to the formation of pores by magainin 2, *Biochemistry 37*, 11856−11863.
8. Oren, Z., and Shai, Y. (1999) Mode of action of linear amphipathic α-helical antimicrobial peptides, *Biopolymers 47*, 451−463.
9. Shai, Y. (1999) Mechanism of the binding, insertion and destabilization of phospholipid bilayer membranes by α-helical antimicrobial and cell non-selective membranes-lytic peptides. *Biochim. Biophys. Acta 1462*, 55−70.
10. Jang, W. S., Kim, K. N., Lee, Y. S., Nam, M. H., and Lee, I. H. (2002) Halocidin: a new antimicrobial peptide from hemocytes of the solitary tunicate, Halocynthia aurantium, *FEBS Lett. 521*, 81−86.

11. Jang, W. S., Kim, C. H., Kim, K. N., Park, S. Y., Lee, J. H., Son, S. M., and Lee, I. H. (2003) Biological activities of synthetic analogs of halocidin, an antimicrobial peptide from the tunicate Halocynthia aurantium, *Antimicrobial Agents Chemother. 47*, 2481−2486.
12. Lee, H. I., Lee, Y. S., Kim, H. C., Kim, C. R., Hong, T., Menzel, L., Boo, L. M., Pohl, J., Sherman, M. A., Waring, A. J., and Lehrer, R. I. (2001) Dicynthaurin: an antimicrobial peptide from hemocytes of the solitary tunicate, *Halcynthia auranthium*. *Biochim. Biophys. Acta 1527*, 141−148.
13. Wen, S., Majerowicz, M., Waring, A., Lehrer, R., and Bringezu, F. (2006) Dicynthaurin Monomer Interaction with Phospholipid Bilayers: Binding and Pore Formation as Studied by Leakage and Calorimetry, *J. Phys. Chem. B*, accepted.
14. Hristova, K., Dempsey, C. E., and White, S. H. (2001) Structure, Location, and Lipid Perturbations of Melittin at the Membrane Interface, *Biophys. J. 80*, 801−811.
15. Vogel, H. (1987) Comparison of the conformation and orientation of alamethicin and melittin in lipid membranes, *Biochemistry 26*, 4562−4572.
16. Vogel, H., Jähnig, F., Hoffmann, V., and Stümpel, J. (1983) The orientation of melittin in lipid membranes. A polarized infrared spectroscopy study, *Biochim. Biophys. Acta 733*, 201−209.
17. Yang, L., Harroun, T. A., Weiss, T. M., Ding, L., and Huang, H. W. (2001) Barrel-Stave Model or Toroidal Model? A Case Study on Melittin Pores, *Biophys. J. 81*, 1475−1485.
18. Mak, D. O. D., and Webb, W. W. (1995) Two classes of alamethicin transmembrane channels: Molecular models from single-channel properties, *Biophys. J. 69*, 2323−2336.
19. Duclohier, H., Molle, G., and Spach, G. (1989) Antimicrobial peptide magainin I from Xenopus skin forms anion-permeable channels in planar lipid bilayers, *Biophys. J. 56*, 1017−1021.
20. Ludtke, S. J., He, K., Heller, W. T., Harroun, T. A., Yang, L., and Huang, H. W. (1996) Membrane pores induced by magainin, *Biochemistry 35*, 13723−13728.
21. Majerowicz, M., Waring, A., Wen, S., and Bringezu, F. (2007) Interaction of the antimicrobial peptide Cynthaurin with membrane phospholipids at the air-liquid interface, *J. Phys. Chem. B 111*, 3813−3821.
22. Bringezu, F., Majerowicz, M., Maltseva, E., Wen, S., Brezesinski, G., and Waring, A. (2006) Penetration of the Antimicrobial Peptide Cynthaurin into Phospholipid Monolayers at the Liquid/Air Interface, *ChemBioChem*, accepted.
23. Binder, H., and Lindblom, G. (2003) Interaction of the Trojan peptide penetratin with anionic lipid membranes—a calorimetric study, *Phys. Chem. Chem. Phys. 5*, 5108−5117.
24. Beschiaschvili, G., and Seelig, J. (1990) Peptide binding to lipid bilayers. Binding isotherms and zeta-potential of a cyclic somatostatin analogue, *Biochemistry 29*, 10995−11000.
25. Franks, N. P., and Lieb, W. R. (1979) The structure of lipid bilayers and the effects of general anaesthetics. An x-ray and neutron diffraction study, *J. Mol. Biol. 133*, 469−500.
26. Bradshaw, J. P., Davies, S. M. A., and Hauss, T. (1998) Interaction of Substance P with Phospholipid Bilayers: A Neutron Diffraction Study, *Biophys. J. 75*, 889−895.
27. Dante, S., Hauss, T., and Dencher, N. A. (2003) Insertion of externally administered amyloid beta peptide 25−35 and perturbation of lipid bilayers, *Biochemistry 42*, 13667−13672.
28. Wieprecht, T., Beyermann, M., and Seelig, J. (1999) Binding of antibacterial magainin peptides to electrically neutral membranes: thermodynamics and structure, *Biochemistry 38*, 10377−10387.
29. Tanford, F. (1980) *The hydrophobic effect: formation of micelles and biological membranes*, Wiley & Sons, New York.
30. Seelig, A., and Ganz, P. (1991) Nonclassical hydrophobic effect in membrane binding equilibria, *Biochemistry 30*, 9354−9359.
31. Sreerama, N., and Woody, R. W. (2004) On the analysis of membrane protein circular dichroism spectra, *Protein Sci. 13*, 100−112.
32. Sreerama, N., and Woody, R. W. (2000) Estimation of protein secondary structure from circular dichroism spectra: comparison of CONTIN, SELCON, and CDSSTR methods with an expanded reference set, *Anal. Biochem. 287*, 252−60.
33. Park, K., Perczel, A., and Fasman, G. D. (1992) Differentiation between transmembrane helices and peripheral helices by the deconvolution of circular dichroism spectra of membrane proteins, *Protein Sci. 1*, 1032−1049.
34. Bowen, M., and Brunger, A. T. (2006) Conformation of the synaptobrevin transmembrane domain, *Proc. Natl. Acad. Sci. U.S.A. 103*, 8378−8383.
35. Dörfler, H. D., and Brezesinski, G. (1983) Phasenumwandlungserscheinungen in Lecithin/Wasser Systemen, *Colloid Polym. Sci. 261*, 286−292.
36. Zhao, W., Rog, T., Gurtovenko, A. A., Vattulainen, I., and Karttunen, M. (2006) Atomic-scale structure and electrostatics of anionic POPG lipid bilayers with Na^+ counterions, *Biophys. J.* 10.1529/biophysj.106.086272.
37. Lindahl, E., Hess, B., and van der Spoel, D. (2001) GROMACS 3.0: a package for molecular simulation and trajectory analysis, *J. Mol. Model. 7*, 306−317.

BI7001295